Effect of graphene and fabrication technique on the release kinetics of carvacrol from polylactic acid.

Roberto Scaffaro*, Andrea Maio, Francesco Lopresti

University of Palermo, Dipartimento di Ingegneria Civile, Ambientale, Aerospaziale, dei Materiali, UdR INSTM di Palermo, Viale delle Scienze Ed. 6, 90128 Palermo, Italy

*Corresponding author. Mail: roberto.scaffaro@unipa.it. Tel: +39.09123863723

Abstract

Porous membranes and thin films containing poly-lactic acid (PLA), carvacrol (CRV) and graphene nanoplatelets (GNP) were fabricated by electrospinning and solvent casting at different formulations.

The systems were characterized from a mechanical, morphological, calorimetric and spectroscopic point of view. CRV release as a function of time was studied and a mathematical model was used to fit and interpret the data in order to investigate the release mechanism.

The results indicate that the incorporation of GNP generally determined a simultaneous strengthening, stiffening and toughening effect, while preserving a good ductility. Furthermore, integrating GNP allowed tuning the amount and kinetics of CRV release, and proved to reduce the initial burst release effect.

Keywords: Electrospinning; Solvent casting; Controlled release; Essential oil; Graphene

1. Introduction

Carvacrol (CRV), an essential oil obtained from oregano, is an aromatic compound belonging to monoterpenoids [1,2]. Owing to its intriguing pharmacological properties, such as antifungal, antibacterial, antioxidant, anticancer activity, CRV attracted significant interest as additive for the formulation of polymer-based materials for food packaging and tissue engineering [1,3,4]. Polylactic acid (PLA) is among the most widespread biodegradable plastics, due to its high mechanical performance, biodegradability, compostability and biocompatibility that enable its use in several application fields, such as food packaging, tissue engineering, and smart delivery [5–9]. The system PLA-CRV is gaining a rising interest in biomedicine owing to the possibility to provide the resulting biomaterials with the natural antibacterial activity of CRV, which allows minimizing the risk of infection after surgery [10]. In a previous work, we demonstrated the possibility to incorporate different amounts of CRV in electrospun membranes based on PLA [11]. In particular, it was found that the release behaviour in PBS of those membranes showed a strong initial burst, with almost 60% of CRV being delivered within the first five hours. In order to mitigate the burst effect, it is usually preferable adding a third component, such as a filler. In fact, from a physical point of view, the presence of a filler may force the molecules to follow a tortuous path throughout the matrix before reaching the surface [12]. Moreover, from a chemical point of view the eventual strong interaction between filler and drug may decrease the amount released and the kinetics delivery.

Graphene nanoplatelets (GNP), belonging to graphene-based materials, possess interesting features, in terms of mechanical, electrical, barrier properties, together with a potentially good affinity to terpenoids, due to their planar structure, constituted by sp^2-hybridized carbon atoms [13–17]. A broad-range of interesting applications was recently reported for nanocomposites containing nanocarbons [18–23].

Unfortunately, despite the importance of biomolecules–graphene interactions, a detailed understanding on the adsorption mechanism and features of terpenoids onto the surface of graphene nanoparticle is lacking due to the complexity of biomolecules [3].

Nevertheless, integrating both GNP and CRV into a PLA matrix could bring several advantages. First of all, due to their mutual affinity, CRV could act as a green exfoliant for graphenic nanoplatelets, due to the presence of aromatic rings, alkyl chains and phenol moieties, able to interact with graphene and solvents, respectively.

At the same time, the good affinity between GNP and CRV may provide a controlled release of oil, with interesting perspectives in the field of biomedical devices. Furthermore, adding CRV is expected to increase the ductility of PLA, whose use is often limited by the extreme fragility, whereas the inclusion of GNP may improve elastic modulus and tensile strength [24,25]. Therefore, their combined use may lead to materials with improved toughness [25,26].

In the frame of this work, a solvent-based technique was adopted for the fabrication of thin films, whereas electrospinning was used to fabricate non-woven mats constituted by continuous fibers, whose diameters range from micro- to nanometer scale [27]. Aim of this work is to provide detailed processing-structure-property relationships for the system PLA-GNP-CRV with a major focus on the effects of GNP and the preparation techniques on the mechanical and release properties of systems containing PLA and CRV.

2. Materials and methods

2.1 Materials

The PLA adopted in this work is a sample of PLA 2002D purchased by Natureworks, whose main characteristics are: melt flow index (210 °C/2.16 kg) = 6 g/10 min, melting

temperature = 151 °C, Mn=113300 Da, Mw=181600 Da). Graphene nanoplatelets (GNP), trade name xGnP®, Grade C, were supplied by XG Sciences Inc., Lansing, MI, USA. Each particle consists of several sheets of graphene with an average thickness of approximately 10–20 nm, average diameter between 1 and 2 μm, and a specific surface area of about 750 m^2/g. Carvacrol (2-methyl-5-(1-methylethyl)-phenol, purity ≥97 %) was supplied by Sigma Aldrich and used as received without further purification. Chloroform (TCM), Acetone (Ac) phosphate-saline buffer (PBS) reagent grade (>99%) were purchased from Sigma Aldrich.

2.2 Preparation routes

Binary PLA-CRV and ternary PLA-CRV-GNP films were prepared by using solvent casting, whereas nanofibrous membranes were obtained by electrospinning. All of the samples contain PLA as a matrix and 14 wt.% CRV, while differing each other for the content of GNP. The formulations herein investigated are summarized in **Table 1**, where ES and SC series refer to nanofibrous membranes and cast films, respectively. The last number of each codename, instead, indicates the GNP weight content, i.e. 0% (for binary systems), 1.4% and 7%.

Table 1. Formulation of the samples investigated within the frame of this work

Sample	PLA (g)	CRV (g)	GNP (g) pre-dispersed in CRV	GNP (g) pre-dispersed in TCM/Ac	GNP_{total} (g)	TCM (mL)	Ac (mL)	Technique
ES-G0	2	0.325581	-	-	-	13.33	6.67	Electrospinning
ES-G1.4	2	0.035443	0.035443	-	0.035443	13.33	6.67	Electrospinning
ES-G7	2	0.35443	0.035443	0.141772	0.177215	13.33	6.67	Electrospinning
SC-G0	2	0.325581	-	-	-	13.33	6.67	Solvent casting
SC-G1.4	2	0.035443	0.035443	-	0.035443	13.33	6.67	Solvent casting
SC-G7	2	0.35443	0.035443	0.141772	0.177215	13.33	6.67	Solvent casting

In all the cases, a solvent mixing step was used. In the case of binary materials, CRV (0.325581 g) was dissolved in 20 mL of TCM:Ac (2:1 vol), thereafter 2 g of PLA were added to the solution and totally dissolved by stirring overnight. As regards the process for the preparation of ternary systems, **Figure 1**, in a first step a stable dispersion of GNP in CRV (1:10 wt) was achieved by sonicating for 4 hours. At the same time, a metastable suspension of GNP (0.141772 g for materials containing 7% of GNP) in 20 mL of TCM:Ac (2:1 vol) was achieved in the same way. Thereafter, GNP/CRV slurry (containing 0.035443 g of GNP in 0.35443 g of CRV) was added dropwise and finally 2 g of PLA were added (10 wt% with respect to the solvents) in order to obtain the designed formulation and completely dissolved by stirring overnight.

The formulation of the samples containing 1.4 wt% of GNP (ES-G1.4 or SC-G1.4) was achieved by simply adding dropwise GNP/CRV masterbatch to PLA.

The solutions were then either poured in a glass and processed into extremely thin films or transferred into a glass syringe fitted with a 19-gauge stainless steel needle for further electrospinning. In this latter case, a conventional electrospinning equipment (Linari Engineering-Biomedical Division, Italy) was used to prepare nanofibrous membranes, using the following parameters: flow rate, 1 mL/h; distance between the needle tip and the collector, 15 cm; supplied high voltage, 15 kV; temperature, 25 °C and relative humidity, 40%. The nanofibers obtained were collected on a grounded rotary drum (diameter=25 mm, speed=5 rpm), wrapped in an aluminum foil for 90 min in order to obtain membranes of 100 μm thickness. The collected electrospun membranes were subsequently dried for at least 2 days under fume hood in order to remove any residual solvents.

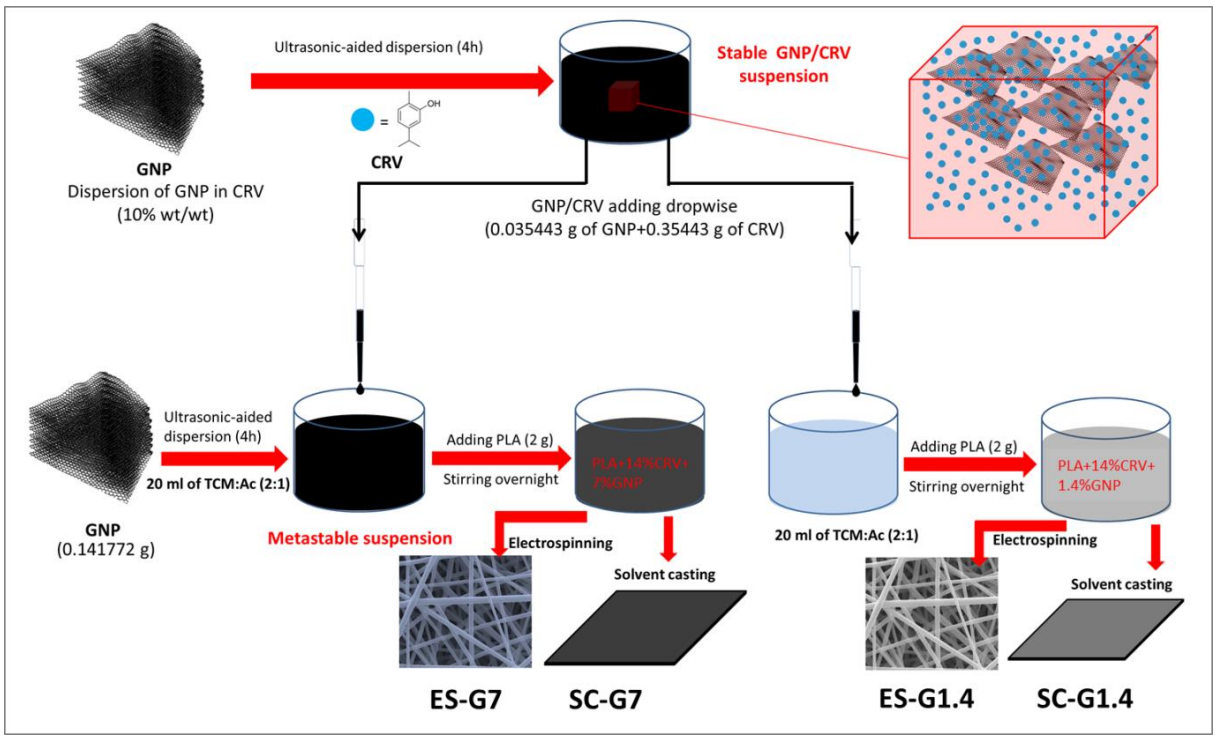

Figure 1. Schematics for the preparation of ternary PLA-CRV-GNP systems

2.3 Characterization techniques

2.3.1 Spectroscopic analysis

The spectroscopic characterization of the samples was performed by FT-IR/ATR analysis, by using a Perkin-Elmer FT-IR/NIR Spectrum 400 spectrophotometer. The spectra were collected in the range 4000–400 cm^{-1}.

2.3.2 Morphological analysis

The morphology of films and nanofibrous mats was evaluated by scanning electron microscopy, SEM (Phenom ProX, Phenom-World). The samples were attached on an aluminum stub using an adhesive carbon tape and then sputter coated with gold (Sputtering Scancoat Six, Edwards) for 90 s under argon atmosphere in order to avoid electrostatic discharge during the test. Fiber diameter distribution was determined using Diameter J, according to our previous works [11,27]

2.3.3 Mechanical testing

Tensile mechanical measurements were carried out by using a dynamometer (Instron model 3365) on rectangular shaped specimens (10 × 90 mm) cut off from the membranes and the films prepared as described above. The tests were performed with a crosshead speed of 1 mm min^{-1} for 2 mm and 50 mm min^{-1} until failure. The distance between the jaws was 30 mm, whereas the thickness was measured before each measurement. Seven samples were tested for each material and the average values and standard deviations were reported. Elastic modulus was then calculated as the slope of stress-strain curve in the initial linear range, whereas toughness was measured as the integrated area of each curve.

2.3.4 Calorimetric analysis

The thermal properties of the systems were analyzed by using a differential scanning calorimeter (DSC), Shimadzu (model DSC-60 Italia s.r.l., Milan, Italy). Specimens, of approximately 10 mg weight, were sealed in aluminum pans. The experiments were performed under N_2 atmosphere with a double cycle of heating from room temperature to 190 °C at 5 °C/min separated by a single cooling run at 5 °C/min.

The degree of crystallinity (χ) of PLA and its composites (calculated considering the amount of PLA according to its weight percentage in the PLA/CRV system) was calculated according to Eq. (1):

$$\chi = \frac{\Delta H_m - \Delta H_{cc}}{\Delta H_m^0} \cdot 100 \qquad (1)$$

where ΔH_{cc} and ΔH_m are, respectively, the cold crystallization enthalpy and the melting enthalpy of the sample. ΔH_m^0 is the melting enthalpy of 100% crystalline PLA (93.7 J/g) [28].

2.3.5 Release kinetics of carvacrol from the polymeric films and membranes

Series of carvacrol solutions of PBS containing 1, thru 20 mg/dL of carvacrol were used to obtain a calibration curve, correlating the absorbance peak intensity and the essential oil concentration using a UV/vis spectrophotometer (model UVPC 2401, Shimadzu Italia s.r.l., Milan, Italy). In the concentration range herein investigated, the calibration curve was found to be a line. The maximum absorbance peak was detected at 273 nm for carvacrol. The release of carvacrol from films and membranes was investigated by immersing a pre-weighed sample (a disk with 25 mm diameter) in 10 mL of PBS. At specific time intervals, the absorbance peak intensity at 273 nm for carvacrol of the storage solutions was measured and converted to the quantities of essential oil released based on the calibration line. After each measurement, the samples were immersed in 10 mL of fresh PBS and the cumulative release of oil was calculated by sequentially adding the oil released after each step.

3. Results and discussion

Chemical-physical characterization of the samples was carried out by FTIR/ATR. In fact, this technique is particularly useful to detect eventual interactions between CRV and GNP, as well as to investigate the structural features of the electrospun fibers.

FTIR/ATR results for GNP, CRV and GNP/CRV dispersion are provided in Figure 1A, together with the digital photographs of GNP dispersions in Chloroform (1 wt.%) and in CRV (10 wt.%) after one week.

Consistently with literature data, GNP modes are weakly IR-active and the spectrum presents a bunch of overlapped bands, which make extremely difficult to distinguish the contribution of each signal [29,30]. By contrast, CRV shows characteristic peaks at 3378 cm^{-1} (OH), 2960 cm^{-1} (CH stretching), 1459 cm^{-1}, 1382 cm^{-1} and 1346 cm^{-1} (CH deformation) and 866 cm^{-1} and 812 cm^{-1} (aromatic ring) [11]. FTIR spectrum of GNP/CRV dispersion presents substantially all the main peaks of CRV. However, some

slight difference can be detected in the range 1700-1400 cm^{-1}, which is related to C=C vibrations [31–33]. A close-up of this spectral region is provided in the inset of the same figure. It can be noted that the band centered at 1502 cm^{-1} in CRV, shifts towards 1499 cm^{-1} with the insurgence of a shoulder centered at 1492 cm^{-1} in CRV/GNP. It was reported for CRV, and in general for π-π stacked organic compounds-graphene structures, that the shifts of ν C=C vibration band components towards lower wavenumbers would indicate an aromatic interaction with graphenic structure [31,32]. This feature could reasonably explain the impressively high dispersability of GNP in CRV, even at higher GNP concentration, whereas their dispersion in TCM was found to be metastable at a concentration as low as 1 wt.%.

Aiming to detect CRV embedded within the polymer matrix, as well as eventual interactions between CRV, GNP and PLA, spectroscopic analysis was carried out onto electrospun fibers, too. **Figure 2B** provides FTIR/ATR spectra of ES-G0 and ES-G7, together with that of neat PLA, taken as reference plot.

With respect to neat PLA, ES-G0 and ES-G7 systems clearly display the typical CRV modes centered at 812 cm^{-1} and 1421 cm^{-1}, respectively ascribed to aromatic ring band and C-H vibration stretching, thus confirming the successful inclusion of the essential oil in the PLA nanofibrous mat. Moreover, even in the C=C aromatic region (1600-1400 cm^{-1}), the same bands previously discussed (Fig. 2A) were recognized for ES-G0 and especially ES-G7.

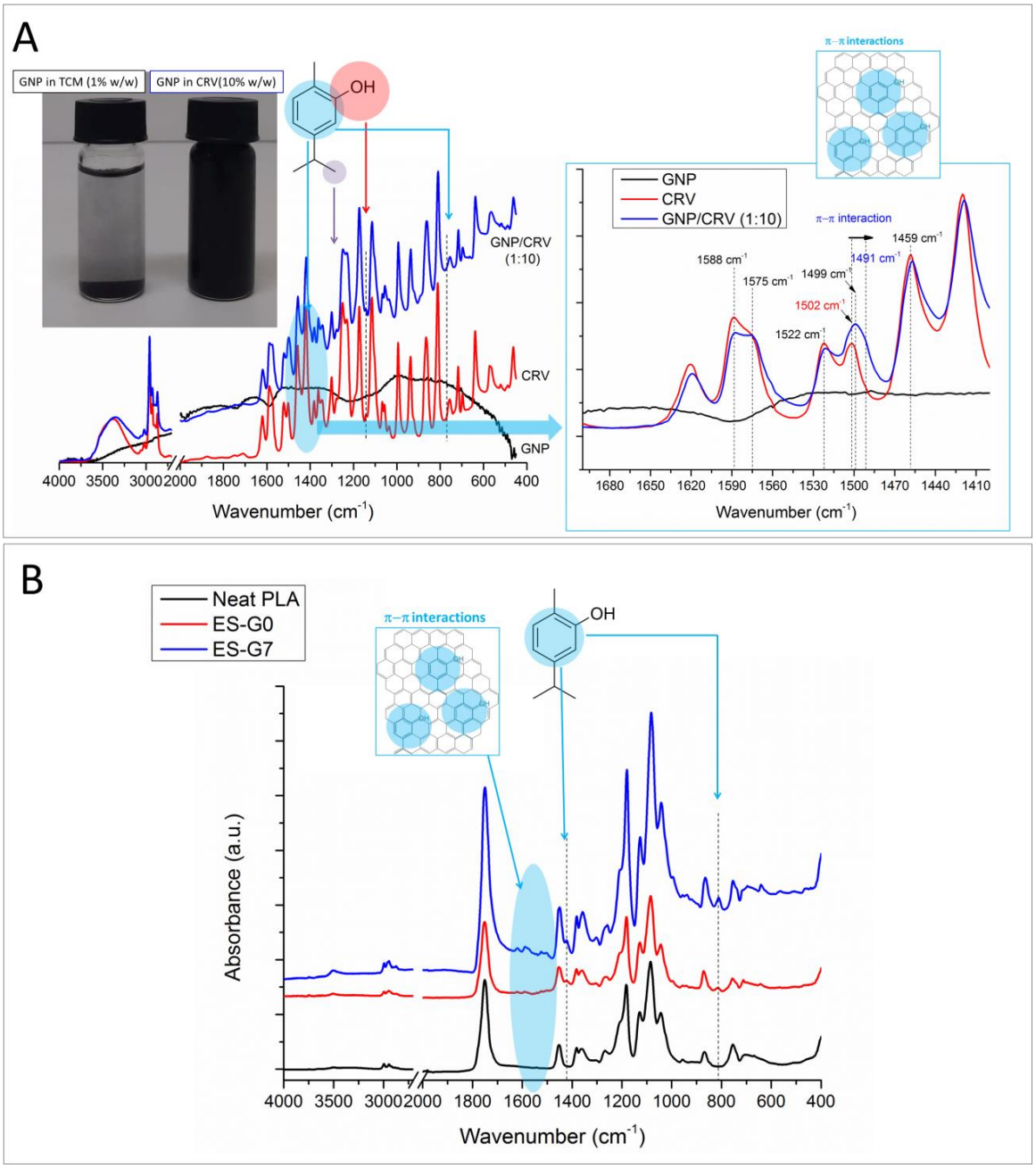

Figure 2. FTIR/ATR spectra of GNP, CRV and GNP/CRV (1:10) together with a digital photograph of dispersability of GNP in TCM and in CRV (A); FTIR/ATR spectra of ES-G0 and ES-G7 together with that of electrospun neat PLA as reference plot (B).

The morphology of ES-series materials is shown in **Figure 3A-C**, together with the analysis of fibers size distribution, reported in **Figure 3 D-E**. Mats are composed by randomly oriented fibers, whose diameters are in the nanoscale range. More in detail, in **Figure 3A** it can be observed that the membranes display homogeneous diameter all

over the surface for PLA-CRV system. Differently, the presence of GNP (**Figs 3 B-C**) progressively increased the irregularity of fiber diameters [34]. The results of fiber diameter distributions in the three samples are provided in **Fig. 3D**. Although all the materials displayed a unimodal distribution with a maximum centered around 1.5 μm, the diameter distribution proved to be quite narrow in the absence of GNP, while broadening upon increasing the ratio between GNP and CRV (G/C ratio). As a result, of course, the weighted average fiber diameter was found to increase upon G/C ratio, **Fig. 3E**.

The morphology of SC-series materials is provided in **Figs 4A-C** that report the micrographs of the cross-sections for SC-G0, SC-G1.4 and SC-G7, respectively. All the samples display the presence of voids, likely due to solvent evaporation. In the absence of GNP, **Fig. 4A,** CRV appears mainly stratified in a layer sandwiched between PLA compact skin and PLA porous core. Adding 1.4% of GNP, **Fig. 4B,** determines a less porous architecture with the presence of aggregates ranging from submicrometric to few microns in size. Incorporating 7% of GNP, **Fig. 4C**, does not prevent particle aggregation and a bad dispersion was found, with particles clusters in the order of tens of micron.

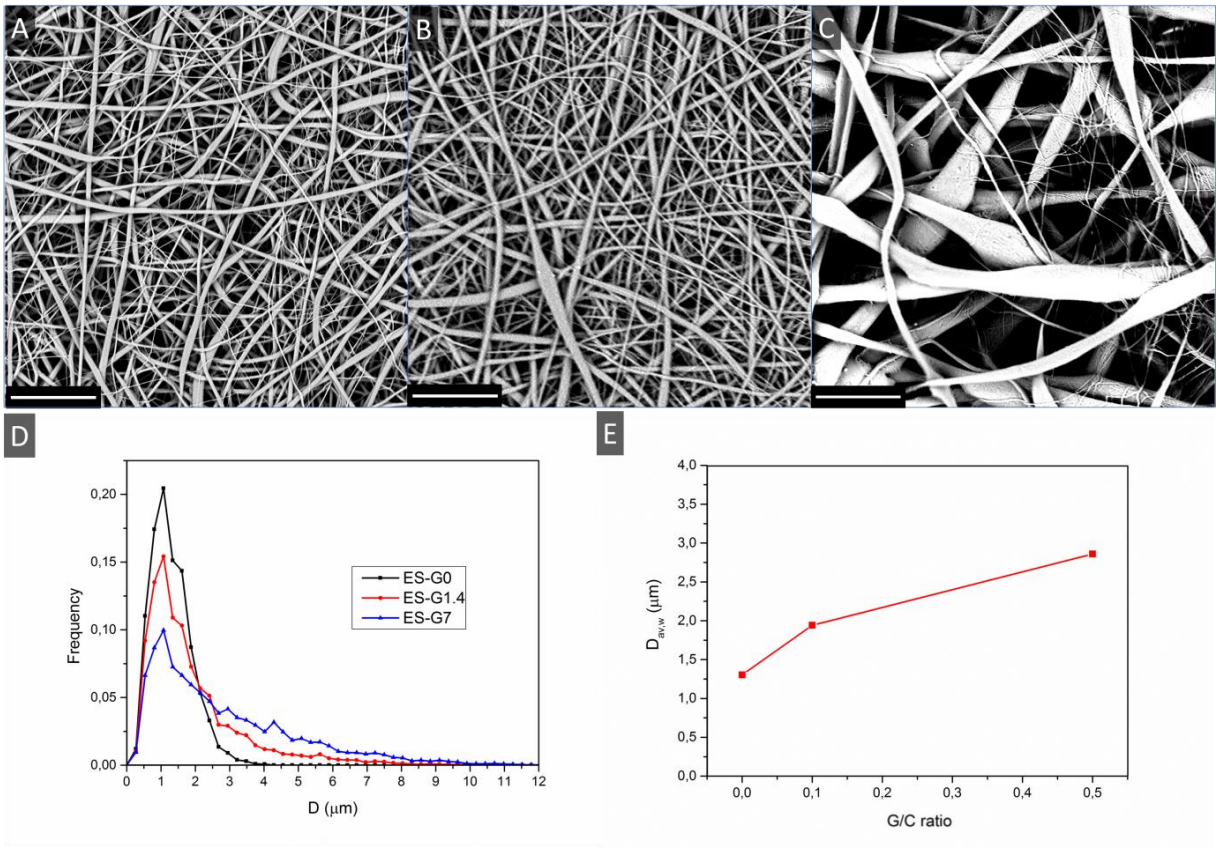

Figure 3. SEM micrographs of ES-G0 (A), ES-G1.4 (B), ES-G7 (C), together with fiber diameter distribution (D) and weighted average values (E). Scale bar=30 µm.

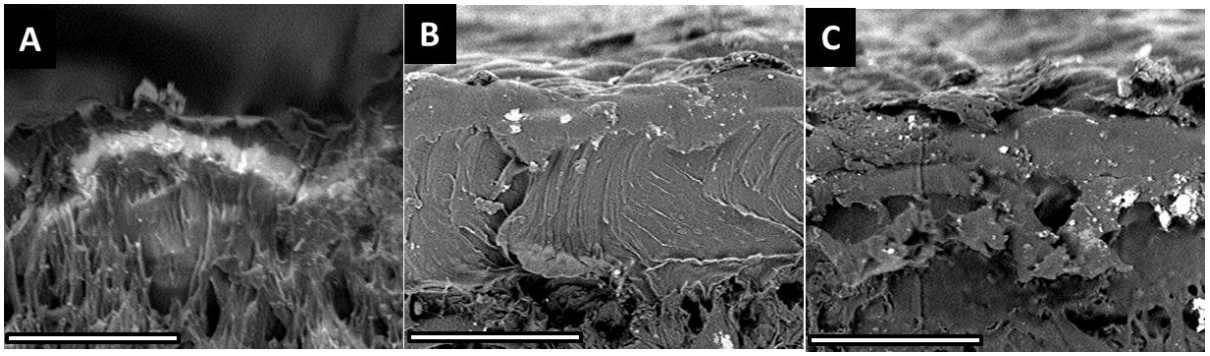

Figure 4. Micrographs of cross section of SC-G0 (A) SC-G1.4 (B), SC-G7 (C). Scale bar=30µm

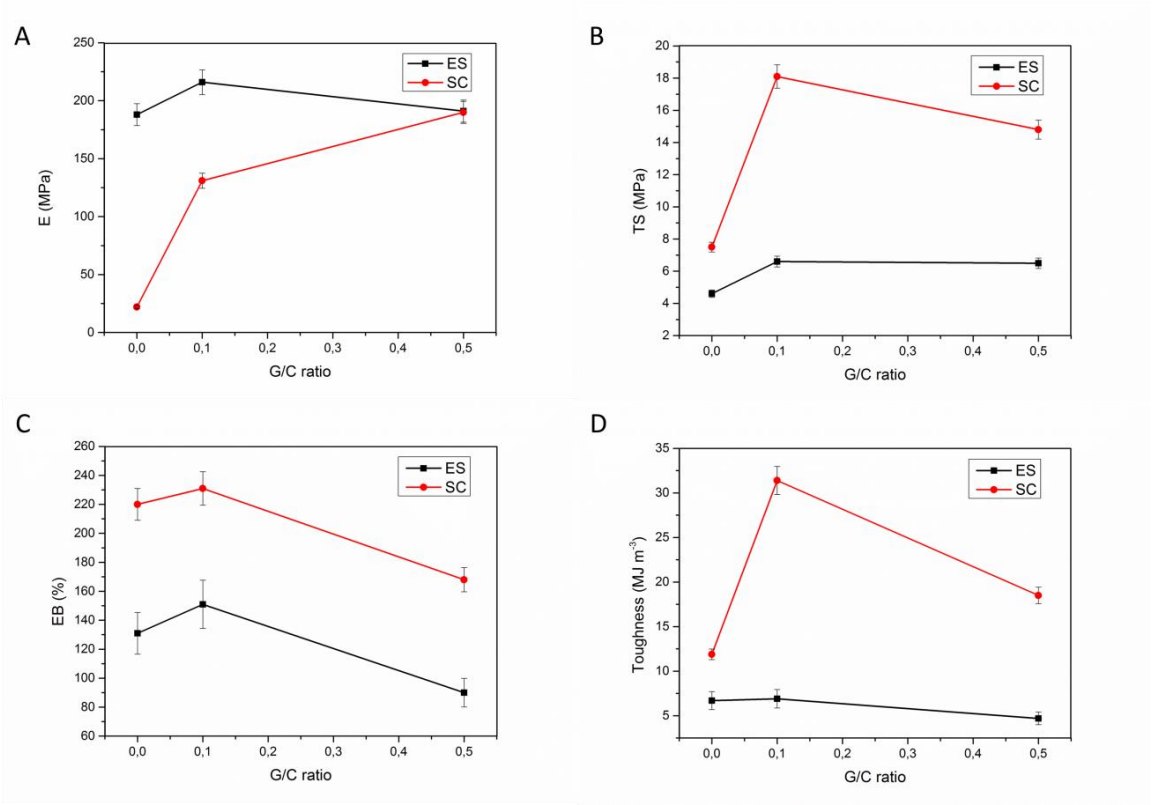

Figure 5. E (A), TS (B), EB (C) and toughness (D) plotted as a function of G/C ratio for ES-series and SC-series materials.

Figure 5 provides the mechanical properties derived from tensile tests, i.e. elastic modulus (E), tensile strength (TS), elongation at break (EB) and toughness, plotted as a function of G/C ratio. First, the ES-series materials were found to be generally stiffer and less stretchable than SC-series samples, with all of the samples displaying however higher values of TS, EB and toughness. Interestingly, the mechanical stiffness of ES-G0 and SC-G0 was found to be substantially different depending on the technique used. In fact, ES-G0 displayed elastic modulus higher than that of SC-G0 [35]. As already studied in our previous work[11], this feature could be presumably explained by taking into account two concurrent phenomena. Indeed, on one hand the low molecular weight CRV can act as a plasticizer thus reducing intermolecular forces of polymer chains. This phenomenon determines a fragile to ductile transition in PLA after CRV incorporation, which leads to a remarkable stretchability with respect to neat PLA, whose EB was

found to be approximately 8% [11], On the other hand, in the case of ES-series samples, the presence of CRV can enhance the surface interactions among the fibers of the mats, thus hindering their slipping and leading to an increase of the elastic modulus, as visible in **Fig. 5A** [11]. The effect of GNP level, i.e. G/C ratio, on E, TS, EB and toughness was found to be different depending on the fabrication technique used. In fact, for ES-series materials, E, Fig. 4A, was found to slightly increase only at low GNP loading (G/C=0.1). This feature can be explained by considering the different architecture of fibrous mats achieved in the three different formulations [36]. In fact, the scarce uniformity of fiber diameters detected especially at high GNP content, presumably led to a worsening of this property, likely due to the lower mechanical resistance of submicrometric fibers and to the presence of defects [37]. Nevertheless, the GNP determined a significant strengthening effect, **Fig. 5B**, independently from G/C ratio used, whereas EB, **Fig. 5C**, was found to follow the same trend observed for E. No remarkable differences were observed for toughness, **Fig. 5D**, although the incorporation of GNP led to a slight decrease of this property.

By contrast, SC-series materials displayed a different behavior, since SC-G0 displayed an elastic modulus as low as 22 MPa, whereas adding 1.4% of GNP determined an elastic modulus of 131 MPa (six-fold higher than SC-G0), and the incorporation of 7% GNP led to an elastic modulus of 190 MPa (i.e. almost nine-fold higher with respect to that of SC-G0). TS was found to be about two-fold than SC-G0 in all the systems containing GNP, regardless of the GNP concentration, as reported for similar systems [38–41]. As regards the stretchability, EB was not altered by the presence of low contents of GNP, whereas the systems loaded with 7% of GNP showed EB values of 165%, significantly lower than SC-G0 and SC-G1.4 which displayed EB values around 220-240%. Adding GNP results in a remarkable toughening effect, especially for G/C=0.1 (+280% increment).

Figure 6 reports the cumulative release of CRV expressed as M_t/M_∞ ratio upon immersion time, where M_t refers to the amount of CRV released at time t, and M_∞ represents the theoretical amount of CRV incorporated in the samples. All the curves display an initial burst zone, followed by a rapid or progressive leveling off, depending on technique and formulation. In fact, the preparation technique has a strong influence on the release behavior of the systems, since electrospun membranes display M_t/M_∞ values higher than the corresponding formulations prepared by solvent casting, expectedly due to the higher surface area of membranes with respect to films.
The fraction of CRV entrapped in the systems prepared, M_{en}, was easily calculated as (eqn. 2):

$$M_{en} = 1 - M_F/M_\infty \quad (2)$$

Where M_F is the amount released at the end of experiment.

Indeed, M_{en} mainly depends on the porosity of devices, in fact ES-series samples display extremely low values of M_{en} with respect to the corresponding SC-series. Furthermore, it increases upon G/C ratio and it is likely due to the strong interaction between GNP and CRV, as visible in **Fig. 7**.

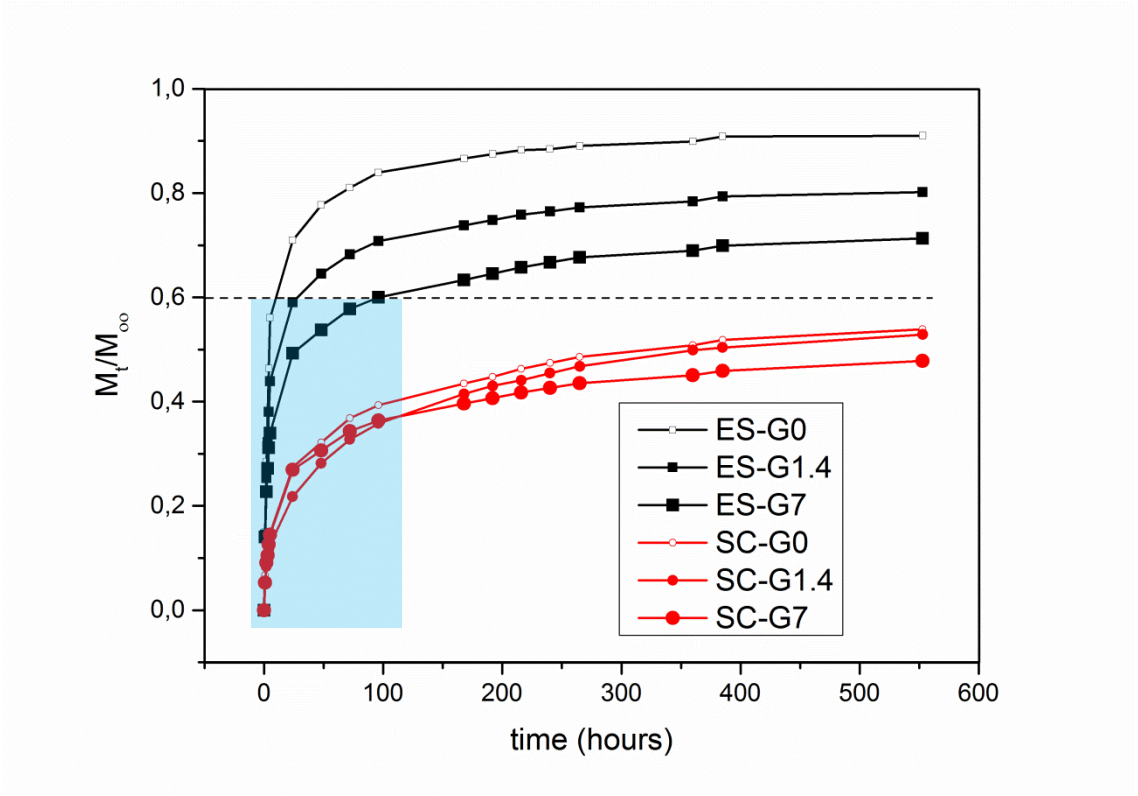

Figure 6. Cumulative CRV release as a function of time from the samples investigated.

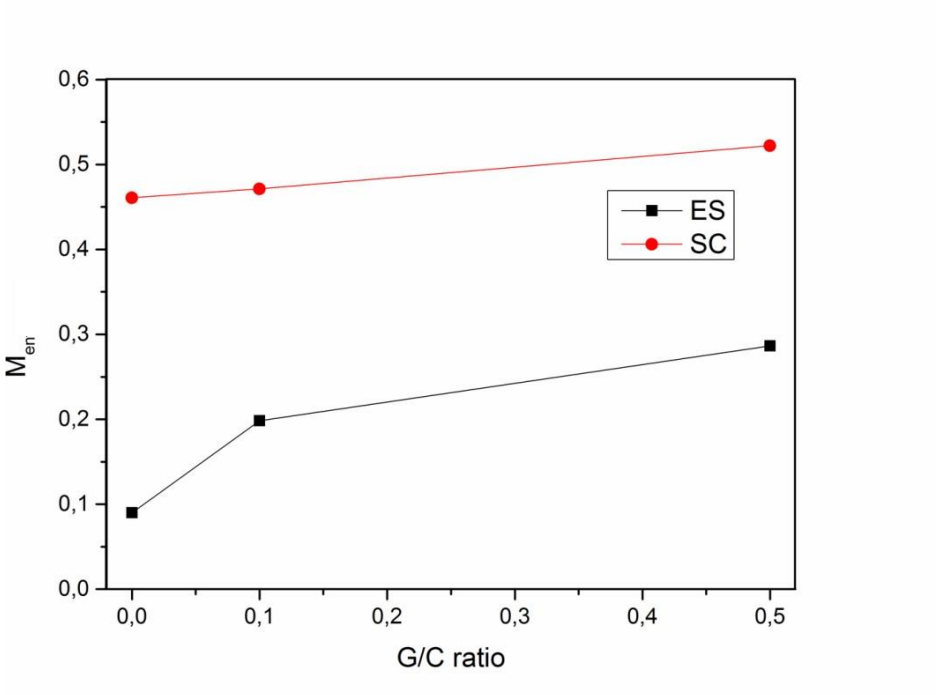

Figure 7. M_{en} plotted as a function of G/C ratio for ES-series and SC-series systems.

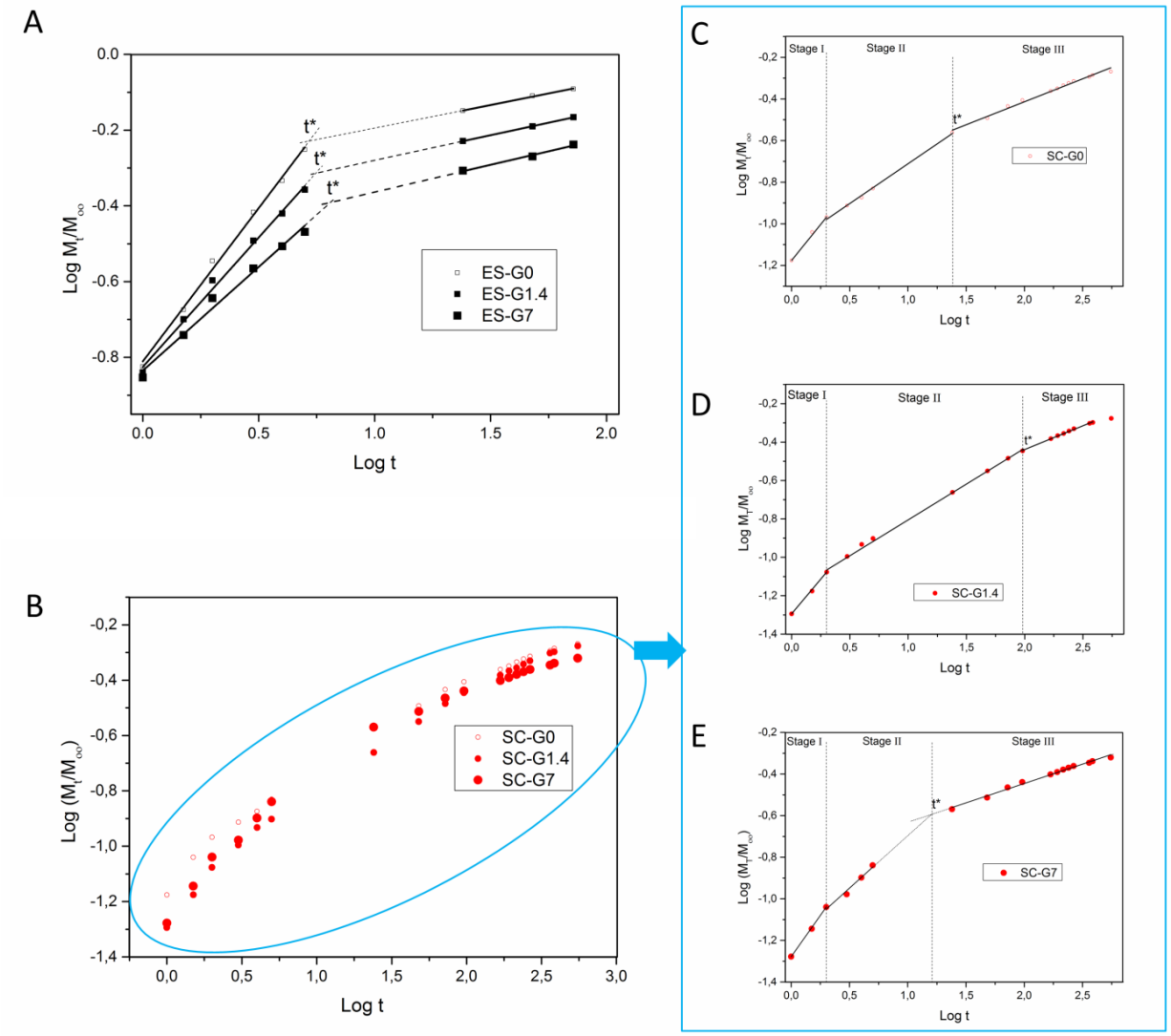

Figure 8. Power law model applied to the release data of ES-series (A), SC-series (B). For sake of clarity, linearization of SC-G0 (C), SC-G1.4 (D) and SC-G7 (E) are provided as separated plots.

Table 2. Release data achieved by linear fitting the plots

Sample	Burst release			Sustained release			Slow release		
	n	k	R^2	n	k	R^2	n	k	R^2
ES-G0	0.8097	0.1545	0.994	-	-	-	0.1222	0.4820	0.998
ES-G1.4	0.6835	0.1494	0.997	-	-	-	0.1315	0.3884	0.999
ES-G7	0.5478	0.1461	0.980	-	-	-	0.1424	0.3125	0.999
SC-G0	0.6922	0.0666	0.999	0.3820	0.0806	0.997	0.2205	-0.8545	0.989
SC-G1.4	0.7223	0.0508	0.999	0.3719	0.0673	0.996	0.2472	-0.9328	0.998
SC-G7	0.6102	0.0549	0.999	0.5069	0.0628	0.975	0.1862	-0.8180	0.991

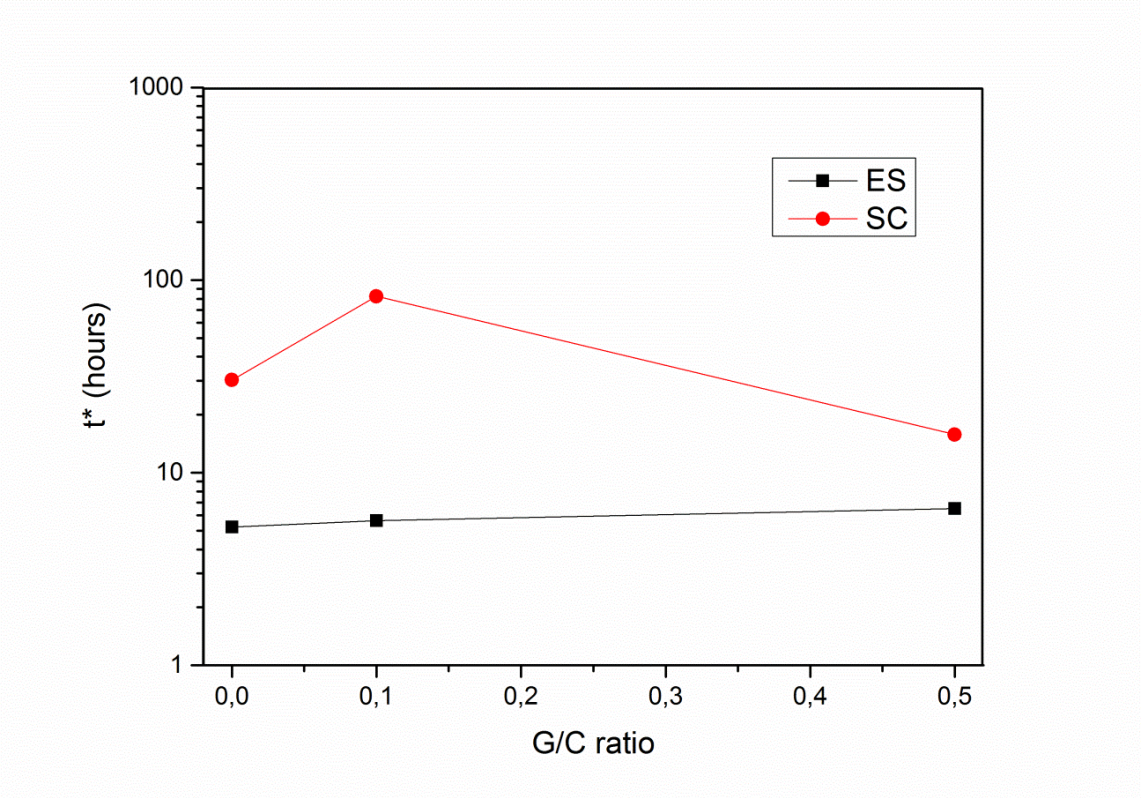

Figure 9. t* plotted as a function of G/C ratio for ES- and SC-series systems.

The presence and the content of GNP affected the release behaviour, too. Regardless from the preparation techniques, the higher the GNP content, the lower the final value of M_T/M_{∞}. This finding can be reasonably ascribed to the aromatic interactions between GNP and CRV that hinder the diffusion of some molecules, as well as to the tortuous path that CRV molecules have to follow throughout the matrix to reach the surface. However, in the SC-series materials it can be noted that M_t/M_{∞} plots of SC-G1.4 and SC-G7 intersect each other at around 100 hours. That is, SC-G7 shows release kinetics faster than SC-G1.4 for t<100 h, thereafter a trend reversal is observed. Hence, it can be hypothesized that adding GNP at low content results in slow diffusion in the first hours but it does not alter the final amount of CRV released. High loading levels of GNP increase the kinetics at the initial stages while dramatically decreasing the release kinetics in the final stages, thus decreasing the final amount of CRV delivered. To get further insight the diffusion mechanism, the experimental data were reported by plotting

log M_t/M_∞ versus log time and fitted with the well-known power law, according to Peppas model [42–45]:

$$\frac{M_t}{M_\infty} = kt^n \qquad (3)$$

Where t is the release time, k is a kinetic constant related to the properties of the drug delivery system, and n is the diffusion exponent that is an indicator about the release mechanism. In particular, when n is lower than 0.5 the drug release is Fickian, i.e. governed by diffusive phenomena, whereas it is dominated by swelling phenomena when n is equal to 1.0. Values of n between 0.5 and 1.0 indicate the so-called anomalous transport, being characterized by the combination of both phenomena. The Peppas model, however, is valid only for $M_t/M_\infty<0.6$ [46]. Therefore, in the case of ES-series material, this model can be applicable only in the early portion of the release curves, whereas it is able to describe the whole delivery mechanism of SC-series samples. The release data were fitted by using equation (3) but splitting them into different time intervals, aiming at finding a satisfactory value of R^2.

Fig. 8A provides the log M_t/M_∞ versus log time plots of ES-series materials, whereas the results of power model law fitting are reported in **Table 2**. In this case, two distinctive release phases were individuated, i.e. an initial burst stage, followed by a slow drug release process.

In the case of SC-series samples, **Fig. 8B**, log M_t/M_∞ vs Log t plots, were found to overlap, and the results of power law fitting are provided as individual plots in **Figs 8D-F**, for sake of clarity. It can be observed that in this case, the best fitting (whose results are reported in **Table 2**) is achieved by dividing the plots into three time intervals: an initial burst release (with all the sample exhibiting $n>0.5$), a sustained release ($0.38<n<0.51$), a slow release (with $n<0.25$). It can be noted that in the initial part of release , the diffusion process prevalently observed is a combination of Fickian

(stochastic diffusion) and non-Fickian diffusion (relaxation phenomenon involved in mass diffusion), and is known as anomalous diffusion. It occurs for all the SC-series systems and it is scarcely affected by G/C ratio. On the other hand, n was found to decrease upon increasing G/C ratio for ES-series systems and in particular the diffusion mechanism of ES-G7 proved to be Fickian, likely due to a higher resistance towards the solvent penetration imparted by the presence of hydrophobic nanoparticles. The values of n calculated in the middle part of release are lower than 0.5 for all the systems, except SC-G7, where a Fickian release was observed. In this stage, G/C=0.1 allows a prolonged and more controlled release of CRV.

A fundamental prerequisite of the devices for controlled release is to provide a long-term sustained delivery of the target compound after the so-called burst zone [47–49]. In fact, after a certain time interval, the release is found to be too slow and low amounts of CRV are released in the PBS medium. This issue may affect the efficiency of the drug delivery system (e.g. its antibacterial or antitumor activity in the case of CRV). For this purpose, we calculated the intersections between the fitted lines of the sustained release stage and those of slow release stage, i.e.: where the amounts of CRV released are too much low to provide bioactivity and the release curves are in proximity of plateau [50]. Being t* the abscissa of such intersections, this parameter gives useful information about the time release efficiency of these systems. High values of t* indicate a prolonged efficacy of the drug delivery system. **Figure 9** provides the behavior of t* as a function of preparative and formulation.

Expectedly, ES-series materials displayed t* values much lower than SC-series ones. However, for the former ones, t* proved to slightly increase upon increasing G/C. Differently, as regards SC-series, t* was found to be 30 hours for SC-G0, 100 hours for SC-G1.4 and 20 hours for SC-G7. These remarkable differences put into evidence that in bulky materials the structure plays a key-role, being capable to prolong the release

efficiency of a drug delivery device (from 1 day to 4 days) by adding 1.4% GNP. Otherwise, in ES-series materials the improvements achieved by integrating GNP in PLA-CRV structures (i.e. 16-17% relative increase) are still inadequate to ensure a prolonged drug release. Finally, for SC-series materials the state of dispersion exerted a crucial effect on release properties, since adding an extremely high content of GNP gave rise to the presence of micro-sized aggregates, thus creating preferential pathways for the CRV molecules to be diffused out of the matrix. As regards ES-series mats, the presence of GNP affected the distribution of fibers diameters with obvious repercussions on random walk of the diffusing molecules which is supposed to dramatically increase in the case of thicker fibers. Interestingly, a strong correlation can be found between the trend followed by mean fiber diameter and M_{en} when plotted as a function of G/C ratio.

Anyhow, beyond dispersion, adhesion, chemical affinity between GNP and CRV, another key-factor that can affect the diffusive phenomena is the crystallinity of the matrix, which may determine a decrease of diffusive kinetics [12,42].

DSC results are reported in **Table 3**. As one can see, all the materials are practically amorphous, as typically expected, and no glass transition was recognized [11]. The former feature demonstrates that the different release behavior is not governed by changes in crystallinity, whereas the latter feature suggests that CRV acts as a plasticizer for PLA, which turns from a glassy to a rubbery behavior at room temperature, and explains the high stretchability observed during mechanical tests for all the materials. Moreover, as regards the films, the presence of GNP increased T_{CC}, whereas melting temperature was found to be unaffected by the presence of the filler and located at around 150 °C. As concerns the ES-series, cold crystallization phenomena were recognized at T lower than the corresponding SC-films, but practically

unaffected by the presence of GNP. However, in this latter case the melting temperature was found to decrease upon increasing G/C ratio.

It can be concluded that being crystallinity not significantly different for all ES-series and SC-series materials, it does not play a relevant role in affecting the release kinetics, which seems to be mainly governed by fiber diameter mean size for ES-series samples and by dispersion state of GNP for SC-series materials.

Table 3. DSC results of the samples investigated

Sample	T_g[°C]	T_{cc} [°C]	T_m[°C]	ΔH_{cc} [J/g]	ΔH_m [J/g]	χ [%]
ES-G0	-	83	145	5.3	6.2	1
ES-G1.4	-	82	143.0	4.0	7.7	3.9
ES-G7	-	81.7	140.7	6.4	9.1	2.8
SC-G0	-	85.4	149.9	19.9	23.3	3.6
SC-G1.4	-	92.9	150.2	13.8	19.2	5.8
SC-G7	-	92.0	150.8	19.1	23.1	4.3

4. Conclusion

Membranes and thin films containing poly-lactic acid (PLA), carvacrol (CRV) and graphene nanoplatelets (GNP) were fabricated by electrospinning and solvent casting at different formulations. The effect of GNP and of the technique on the mechanical and release properties of these systems were investigated. More in detail, the release kinetics of CRV in phosphate buffered solution at 37 °C was monitored via UV-Vis measurements and the data were fitted with a power law model. The results of mechanical testing indicated that in the films prepared by solvent casting, the incorporation of GNP determined a simultaneous strengthening, stiffening and toughening effect, while preserving a good ductility. As concerns the membranes, instead, the successful incorporation of CRV and GNP in the polymer matrix damaged the fibers morphology, therefore the stiffness of the nanomats were found to decrease whereas tensile strength proved to increase upon GNP content. As regards the release tests, the power law model put into evidence that the mechanism of CRV release

changed upon time from an anomalous release in the first hours to a Fickian diffusion mechanism for all the systems. Integrating GNP allows tuning the amount and kinetics of CRV release. The mechanism seems to be governed by the type of structure achieved and by the strong interaction between CRV and GNP.

The possibility to modulate the release behaviour by changing formulation and structure (i.e. preparation technique) suggests that preparing multi-layered devices with different structures by gathering different techniques and formulations may ensure a long-term sustained release, suitable for meeting the needs of different areas of biomedicine. Future developments of this work may involve the possible use of these materials in a broad-range of application fields. In fact, nanofibrous membranes based on PLA, GNP and CRV could serve as wound healing devices or as scaffolds for neuronal tissue engineering, owing to the ability of nanocarbons in stimulating neuronal cells growth, while carvacrol is crucial to minimize the risk of infections after surgery.

Cast films containing GNP and CRV could be promising for the realization of sensors and biosensors or for antistatic packaging, due to their extremely enhanced stretchability.

References

[1] A. Nostro, R. Scaffaro, M. D'Arrigo, L. Botta, A. Filocamo, A. Marino, et al., Study on carvacrol and cinnamaldehyde polymeric films: Mechanical properties, release kinetics and antibacterial and antibiofilm activities, Appl. Microbiol. Biotechnol. 96 (2012) 1029–1038. doi:10.1007/s00253-012-4091-3.

[2] A. Ben Arfa, S. Combes, L. Preziosi-Belloy, N. Gontard, P. Chalier, Antimicrobial activity of carvacrol related to its chemical structure, Lett. Appl. Microbiol. 43 (n.d.) 149–154. doi:10.1111/j.1472-765X.2006.01938.x.

[3] H. Deka, M.D. Saikia, H.K. Srivastava, Adsorption of Various Monoterpenoids on the Surface of Graphene and Nitrogen-Doped Graphene: A DFT Based Study, ChemistrySelect. 2 (2017) 5248–5258. doi:10.1002/slct.201700844.

[4] S. Tunç, O. Duman, Preparation of active antimicrobial methyl cellulose/carvacrol/montmorillonite nanocomposite films and investigation of carvacrol release, LWT - Food Sci. Technol. 44 (2011) 465–472. doi:https://doi.org/10.1016/j.lwt.2010.08.018.

[5] R. Scaffaro, A. Maio, G. Lo Re, A. Parisi, A. Busacca, Advanced piezoresistive sensor achieved by amphiphilic nanointerfaces of graphene oxide and biodegradable polymer blends, Compos. Sci. Technol. 156 (2018) 166–176. doi:https://doi.org/10.1016/j.compscitech.2018.01.008.

[6] R. Scaffaro, F. Lopresti, L. Botta, Preparation, characterization and hydrolytic degradation of PLA/PCL co-mingled nanofibrous mats prepared via dual-jet electrospinning, Eur. Polym. J. 96 (2017) 266–277. doi:10.1016/j.eurpolymj.2017.09.016.

[7] R. Scaffaro, F. Lopresti, A. Sutera, L. Botta, R.M. Fontana, G. Gallo, Plasma modified PLA electrospun membranes for actinorhodin production intensification in Streptomyces coelicolor A3(2) immobilized-cell cultivations, Colloids Surfaces B Biointerfaces. 157 (2017) 233–241. doi:10.1016/j.colsurfb.2017.05.060.

[8] R. Scaffaro, F. Lopresti, A. Maio, F. Sutera, L. Botta, Development of polymeric functionally graded scaffold: a brief review, J. Appl. Biomater. Funct. Mater. 15 (2017) 107–121. doi:10.5301/jabfm.5000332.

[9] Y. Li, T. Jing, G. Xu, J. Tian, M. Dong, Q. Shao, et al., 3-D magnetic graphene oxide-magnetite poly(vinyl alcohol) nanocomposite substrates for immobilizing enzyme, Polymer (Guildf). 149 (2018) 13–22. doi:https://doi.org/10.1016/j.polymer.2018.06.046.

[10] J. Lin, X. Chen, C. Chen, J. Hu, C. Zhou, X. Cai, et al., Durably Antibacterial and Bacterially Antiadhesive Cotton Fabrics Coated by Cationic Fluorinated Polymers, ACS Appl. Mater. Interfaces. 10 (2018) 6124–6136. doi:10.1021/acsami.7b16235.

[11] R. Scaffaro, F. Lopresti, Processing, structure, property relationships and release kinetics of electrospun PLA/Carvacrol membranes, Eur. Polym. J. 100 (2018) 165–171. doi:10.1016/j.eurpolymj.2018.01.035.

[12] R. Scaffaro, L. Botta, A. Maio, G. Gallo, PLA graphene nanoplatelets nanocomposites: Physical properties and release kinetics of an antimicrobial agent, Compos. Part B Eng. 109 (2017) 139–146. doi:http://dx.doi.org/10.1016/j.compositesb.2016.10.058.

[13] R. Scaffaro, A. Maio, F. Lopresti, L. Botta, Nanocarbons in electrospun polymeric nanomats for tissue engineering: A review, Polymers (Basel). 9 (2017). doi:10.3390/polym9020076.

[14] A. Maio, R. Scaffaro, L. Lentini, A.P. Piccionello, I. Pibiri, Perfluorocarbons–graphene oxide nanoplatforms as biocompatible oxygen reservoirs., Chem. Eng. J. (2017). doi:https://doi.org/10.1016/j.cej.2017.10.032.

[15] H. Liu, M. Dong, W. Huang, J. Gao, K. Dai, J. Guo, et al., Lightweight conductive graphene/thermoplastic polyurethane foams with ultrahigh compressibility for piezoresistive sensing, J. Mater. Chem. C. 5 (2017) 73–83.

doi:10.1039/c6tc03713e.

[16] H. Liu, Y. Li, K. Dai, G. Zheng, C. Liu, C. Shen, et al., Electrically conductive thermoplastic elastomer nanocomposites at ultralow graphene loading levels for strain sensor applications, J. Mater. Chem. C. 4 (2015) 157–166. doi:10.1039/c5tc02751a.

[17] S. Agnello, A. Alessi, G. Buscarino, A. Piazza, A. Maio, L. Botta, et al., Structural and thermal stability of graphene oxide-silica nanoparticles nanocomposites, J. Alloys Compd. 695 (2017) 2054–2064. doi:http://dx.doi.org/10.1016/j.jallcom.2016.11.044.

[18] W. Haikun, H. Xiaoshuai, Q. Lei, Recent Progress on the Metacompoistes with Carbonaceous Fillers, Eng. Sci. 2 (2018) 17–25. doi:10.30919/es8d656.

[19] Y. He, S. Yang, H. Liu, Q. Shao, Q. Chen, C. Lu, et al., Reinforced carbon fiber laminates with oriented carbon nanotube epoxy nanocomposites: Magnetic field assisted alignment and cryogenic temperature mechanical properties, J. Colloid Interface Sci. 517 (2018) 40–51. doi:https://doi.org/10.1016/j.jcis.2018.01.087.

[20] Z. Wu, S. Gao, L. Chen, D. Jiang, Q. Shao, B. Zhang, et al., Electrically Insulated Epoxy Nanocomposites Reinforced with Synergistic Core–Shell SiO<inf>2</inf>@MWCNTs and Montmorillonite Bifillers, Macromol. Chem. Phys. 218 (2017). doi:10.1002/macp.201700357.

[21] Z. Wang, R. Wei, J. Gu, H. Liu, C. Liu, C. Luo, et al., Ultralight, highly compressible and fire-retardant graphene aerogel with self-adjustable electromagnetic wave absorption, Carbon N. Y. 139 (2018) 1126–1135. doi:https://doi.org/10.1016/j.carbon.2018.08.014.

[22] H. Du, C.X. Zhao, J. Lin, J. Guo, B. Wang, Z. Hu, et al., Carbon Nanomaterials in Direct Liquid Fuel Cells, Chem. Rec. 18 (2018) 1365–1372. doi:10.1002/tcr.201800008.

[23] C. Cheng, R. Fan, Z. Wang, Q. Shao, X. Guo, P. Xie, et al., Tunable and weakly negative permittivity in carbon/silicon nitride composites with different carbonizing temperatures, Carbon N. Y. 125 (2017) 103–112. doi:https://doi.org/10.1016/j.carbon.2017.09.037.

[24] M. Zhao, L. Meng, L. Ma, L. Ma, X. Yang, Y. Huang, et al., Layer-by-layer grafting CNTs onto carbon fibers surface for enhancing the interfacial properties of epoxy resin composites, Compos. Sci. Technol. 154 (2018) 28–36. doi:https://doi.org/10.1016/j.compscitech.2017.11.002.

[25] C. Hu, Z. Li, Y. Wang, J. Gao, K. Dai, G. Zheng, et al., Comparative assessment of the strain-sensing behaviors of polylactic acid nanocomposites: reduced graphene oxide or carbon nanotubes, J. Mater. Chem. C. 5 (2017) 2318–2328. doi:10.1039/c6tc05261d.

[26] Z. Wu, H. Cui, L. Chen, D. Jiang, L. Weng, Y. Ma, et al., Interfacially reinforced unsaturated polyester carbon fiber composites with a vinyl ester-carbon nanotubes sizing agent, Compos. Sci. Technol. 164 (2018) 195–203. doi:https://doi.org/10.1016/j.compscitech.2018.05.051.

[27] R. Scaffaro, F. Lopresti, A. Maio, L. Botta, S. Rigogliuso, G. Ghersi, Electrospun PCL/GO-g-PEG structures: Processing-morphology-properties relationships,

Compos. Part A Appl. Sci. Manuf. 92 (2017) 97–107. doi:10.1016/j.compositesa.2016.11.005.

[28] V. Fiore, L. Botta, R. Scaffaro, A. Valenza, A. Pirrotta, PLA based biocomposites reinforced with Arundo donax fillers, Compos. Sci. Technol. 105 (2014) 110–117. doi:10.1016/j.compscitech.2014.10.005.

[29] A. Maio, S. Agnello, R. Khatibi, L. Botta, A. Alessi, A. Piazza, et al., A rapid and eco-friendly route to synthesize graphene-doped silica nanohybrids, J. Alloys Compd. 664 (2016) 428–438. doi:10.1016/j.jallcom.2015.12.137.

[30] A. Maio, D. Giallombardo, R. Scaffaro, A. Palumbo Piccionello, I. Pibiri, Synthesis of a fluorinated graphene oxide--silica nanohybrid: improving oxygen affinity, RSC Adv. 6 (2016) 46037–46047. doi:10.1039/c6ra02585d.

[31] J. Araña, E.P. Melián, V.M.R. López, A.P. Alonso, J.M.D. Rodríguez, O.G. Díaz, et al., Photocatalytic degradation of phenol and phenolic compounds: Part I. Adsorption and FTIR study, J. Hazard. Mater. 146 (2007) 520–528. doi:https://doi.org/10.1016/j.jhazmat.2007.04.066.

[32] M.J. Deka, D. Chowdhury, Tuning Electrical Properties of Graphene with Different π-Stacking Organic Molecules, J. Phys. Chem. C. 120 (2016) 4121–4129. doi:10.1021/acs.jpcc.5b12403.

[33] Z. Hu, D. Zhang, F. Lu, W. Yuan, X. Xu, Q. Zhang, et al., Multistimuli-Responsive Intrinsic Self-Healing Epoxy Resin Constructed by Host–Guest Interactions, Macromolecules. 51 (2018) 5294–5303. doi:10.1021/acs.macromol.8b01124.

[34] A. Tampau, C. González-Martínez, A. Chiralt, Release kinetics and antimicrobial properties of carvacrol encapsulated in electrospun poly-(ε-caprolactone) nanofibres. Application in starch multilayer films, Food Hydrocoll. 79 (2018) 158–169. doi:https://doi.org/10.1016/j.foodhyd.2017.12.021.

[35] X. Guan, G. Zheng, K. Dai, C. Liu, X. Yan, C. Shen, et al., Carbon Nanotubes-Adsorbed Electrospun PA66 Nanofiber Bundles with Improved Conductivity and Robust Flexibility, ACS Appl. Mater. Interfaces. 8 (2016) 14150–14159. doi:10.1021/acsami.6b02888.

[36] Y. Li, B. Zhou, G. Zheng, X. Liu, T. Li, C. Yan, et al., Continuously prepared highly conductive and stretchable SWNT/MWNT synergistically composited electrospun thermoplastic polyurethane yarns for wearable sensing, J. Mater. Chem. C. 6 (2018) 2258–2269. doi:10.1039/C7TC04959E.

[37] R. Scaffaro, F. Lopresti, Properties-morphology relationships in electrospun mats based on polylactic acid and graphene nanoplatelets, Compos. Part A Appl. Sci. Manuf. 108 (2018) 23–29. doi:10.1016/j.compositesa.2018.02.026.

[38] R. Scaffaro, A. Maio, A green method to prepare nanosilica modified graphene oxide to inhibit nanoparticles re-aggregation during melt processing, Chem. Eng. J. 308 (2017) 1034–1047. doi:http://dx.doi.org/10.1016/j.cej.2016.09.131.

[39] A. Maio, R. Fucarino, R. Khatibi, S. Rosselli, M. Bruno, R. Scaffaro, A novel approach to prevent graphene oxide re-aggregation during the melt compounding with polymers, Compos. Sci. Technol. 119 (2015) 131–137. doi:http://dx.doi.org/10.1016/j.compscitech.2015.10.006.

[40] X. Wang, X. Liu, H. Yuan, H. Liu, C. Liu, T. Li, et al., Non-covalently functionalized graphene strengthened poly(vinyl alcohol), Mater. Des. 139 (2018) 372–379. doi:https://doi.org/10.1016/j.matdes.2017.11.023.

[41] C. Wang, M. Zhao, J. Li, J. Yu, S. Sun, S. Ge, et al., Silver nanoparticles/graphene oxide decorated carbon fiber synergistic reinforcement in epoxy-based composites, Polymer (Guildf). 131 (2017) 263–271. doi:https://doi.org/10.1016/j.polymer.2017.10.049.

[42] R. Scaffaro, L. Botta, A. Maio, M.C. Mistretta, F.P. La Mantia, Effect of Graphene Nanoplatelets on the Physical and Antimicrobial Properties of Biopolymer-Based Nanocomposites, Materials (Basel). 9 (2016) 351. doi:10.3390/ma9050351.

[43] N.R. Saha, G. Sarkar, I. Roy, D. Rana, A. Bhattacharyya, A. Adhikari, et al., Studies on methylcellulose/pectin/montmorillonite nanocomposite films and their application possibilities, Carbohydr. Polym. 136 (2016) 1218–1227. doi:https://doi.org/10.1016/j.carbpol.2015.10.046.

[44] L. Keawchaoon, R. Yoksan, Preparation, characterization and in vitro release study of carvacrol-loaded chitosan nanoparticles, Colloids Surfaces B Biointerfaces. 84 (2011) 163–171. doi:https://doi.org/10.1016/j.colsurfb.2010.12.031.

[45] P.L. Ritger, N.A. Peppas, A simple equation for description of solute release II. Fickian and anomalous release from swellable devices, J. Control. Release. 5 (1987) 37–42.

[46] M.V. Dias, M.M. Sousa, B.R.B. Lara, V.M. de Azevedo, N. de Fátima Ferreira Soares, S.V. Borges, et al., Thermal and morphological properties and kinetics of diffusion of antimicrobial films on food and a simulant, Food Packag. Shelf Life. 16 (2018) 15–22. doi:https://doi.org/10.1016/j.fpsl.2018.01.007.

[47] D.B. Raina, D. Larsson, F. Mrkonjic, H. Isaksson, A. Kumar, L. Lidgren, et al., Gelatin- hydroxyapatite- calcium sulphate based biomaterial for long term sustained delivery of bone morphogenic protein-2 and zoledronic acid for increased bone formation: In-vitro and in-vivo carrier properties, J. Control. Release. 272 (2018) 83–96. doi:https://doi.org/10.1016/j.jconrel.2018.01.006.

[48] S.E. Kim, Y.-P. Yun, K.-S. Shim, D.I. Jeon, K. Park, H.-J. Kim, In vitro and in vivo anti-inflammatory and tendon-healing effects in Achilles tendinopathy of long-term curcumin delivery using porous microspheres, J. Ind. Eng. Chem. 58 (2018) 123–130. doi:https://doi.org/10.1016/j.jiec.2017.09.016.

[49] E. Graham-Gurysh, K.M. Moore, A.B. Satterlee, K.T. Sheets, F.-C. Lin, E.M. Bachelder, et al., Sustained Delivery of Doxorubicin via Acetalated Dextran Scaffold Prevents Glioblastoma Recurrence after Surgical Resection, Mol. Pharm. 15 (2018) 1309–1318. doi:10.1021/acs.molpharmaceut.7b01114.

[50] R. Scaffaro, F. Lopresti, M. D'Arrigo, A. Marino, A. Nostro, Efficacy of poly(lactic acid)/carvacrol electrospun membranes against Staphylococcus aureus and Candida albicans in single and mixed cultures, Appl. Microbiol. Biotechnol. 102 (2018) 4171–4181. doi:10.1007/s00253-018-8879-7.